Scilight

Advanced Chemical Process Analysis

https://www.sciltp.com/journals/acpa

Article

Stochastic Dynamics Mass Spectrometric Analysis of Ozone Depletion Reactions of Pharmaceutics

Bojidarka Ivanova

Institute of Environmental Research, University Dortmund, 44221 Dortmund, Germany; bojidarka.ivanova@yahoo.com or b_ivanova@web.de

How To Cite: Ivanova, B. Stochastic Dynamics Mass Spectrometric Analysis of Ozone Depletion Reactions of Pharmaceutics. *Advanced Chemical Process Analysis* **2026**, *2*(1), 1. https://doi.org/10.53941/acpa.2026.100001

Received: 22 October 2025
Revised: 1 January 2026
Accepted: 5 January 2026
Published: 21 January 2026

Abstract: Pharmaceutical xenobiotics at ng·L^{-1} concentration levels occur in environmental aquatics as metabolized or unchanged chemicals, due to human and animal excretion. Wastewater plants treat polluted sewage waters. Despite this, transformed pollutants are released into the environmental aquatics. Ozonation is utilized for therapeutic purposes. It is based on ion-radicals from O_3 and organic matter. Details on the mechanistic aspects of degradation reactions of pharmaceuticals due to ozonation are crucial in elaborating precise kinetic models for real process monitoring and optimizing cleanup technologies used in sludge and wastewater plants. It is relevant to environmental chemistry, chemical engineering, and process control; thus, improving real industrial-scale technologies. This study first applies an innovative stochastic dynamics mass spectrometric model formula to ozonation processes of metronidazole and carbamazepine. It uses ultra-high resolution electrospray ionization mass spectrometry, high-accuracy approaches to quantum chemistry, and chemometrics. The quantification of metronidazole via the innovative formula, thus, assessing relation $D''_{SD} = f(\text{conc.})$, yields excellent performances $|r| = 0.99979$. The mass spectrometric-based structural analysis shows $|r| = 0.93957$. These excellent performances of examining the very complex case of ozonation reaction of metronidazole highlight that the novel stochastic dynamics tool is the only currently available method for processing of mass spectrometric data on fluctuations of low intensity analyte peaks; thus, producing not only exact quantitative, but also 3D molecular structural analysis of species. The reported performances underline the innovative formula as a prospective novel approach to both the fundamental analytical sciences and industry.

Keywords: pharmaceutics; mass spectrometry; chromatography; structural analysis; stochastic dynamics; ozonation; organic matter

1. Introduction

The environmental water is continuously threatened, due to emerging pharmaceuticals and other micro-contaminants [1–3]. It could be attributed to several factors. There is widespread utilization of medications for self-treatment; hospital wastewater, discharges of industrial wastewater, and more. The environmental pollution due to hospitals is a result of the rate of bio-transformation processes of medications in the body, which remain at about 50–90% none metabolized. They are excreted in water via urine and feces. A release of pharmaceutical metabolites into the environment also occurs.

Due to urban fields and population growth, medications are extensively utilized for treating human diseases, thus increasing their availability in the aquatic environment. There is a hazard to ecosystems and human health. The global consumption of antibiotics should be a 67% increase by the year 2030 [4]. A major source of pharmaceuticals in municipal wastewater is hospital waste. It is at about 5−20% [4].

In order to avoid the adverse effects of therapeutics on the human and ecological environment, research efforts are concentrated on elaborating methods for the destruction of medications from wastewater.

Innovations into clean-up technologies for treating pharmaceutical sewage sludge represent an analytical challenge due to its composition. Besides a broad spectrum of harmful organics, there is a high level of soluble inorganics and heavy metal ions [4].

The medications are not entirely removed in the course of biological treatment. The conventional waste water processing plants (WWPPs) eliminate them fractionally at about 50–90% [4]. The non-processed medications and their metabolites contaminate and harm the ecosystems by developing antibiotic-resistant bacteria [5,6] at low analyte concentrations, due to molecular design directed toward significant biological activity at low doses [5].

Therefore, it is of importance to develop effective removal clean-up technologies for pharmaceuticals from wastewater. The European Union has developed an urban wastewater treatment regulatory framework within the Directive (EU) 2024/3019/27.11.2024 [7]. The micro-pollutants involve not only pharmaceuticals, but also pesticides and personal care products [8]. The same is true for pesticides [9].

Advanced oxidation processes are prospective (photo) chemical, (photo) catalytic, and photo electrochemical tools for removing xenobiotics from water.

The advanced oxidation processes (AOPs) have been highlighted as the only viable approach to remove medications from contaminated water under ambient reaction conditions. They allow for destroying pharmaceuticals [1–3].

The AOPs are mainly based on analyte interaction with hydroxyl radicals, with extremely high oxidative power. Among AOPs, reactions involving ozone achieve a high concentration of $^{\bullet}$OH radical via various pathways. Innovations into theoretical methods, design, and predicting conversion levels of pharmaceutics in AOPs. They could be studied via both experimental and theoretical methods for kinetics. The models require knowledge of rate equations; gas- and water phase flow types, and more. It is crucial in developing effective ozone-based AOP technologies.

An in-depth understanding of the mechanistic aspects and kinetics of processes of the reaction zone in water near the gas-water interface or in bulk water is of importance for reliably determining rate equations. The variation of reaction kinetics of ozone interaction with pharmaceutics depends on chemical and mass transfer rates. Frequently, kinetic models of such reactions are considered slow. Thus, only AOPs in bulk solution are considered. Despite this, there are fast processes, as well. The processes occur not only in bulk solution, but also near the gas–water interface. In the latter cases, if any, the mass balances that do not consider near gas–water interface reactions yield poor results.

The industrial-scale technology of AOPs in pharmaceutics reduces processes to the most effective one. In parallel, the beneficial reaction path, amongst others, requires known and accurate kinetic equations. Only significant accuracy allows reliable conclusions on reaction processes. Developments of accurate kinetic models of therapeutic reactions aim at industrial scale implementing into advanced environmental clean-up technologies. However, these tasks are incapable of going beyond theoretical explanation of processes and failed in modeling accurate kinetics in cases of a lack of precise quantitative and 3D molecular structural data on interacting species.

In the latter context, analytical mass spectrometry, as an irreplaceable quantitative and structural method for analysis of molecules, produces reaction kinetics, as well. It has found a broad spectrum of interdisciplinary applications to many sub-fields of the science; for instance, analytical and environmental chemistry; petroleum chemistry; clinical diagnostics and laboratory medicine; biochemistry, drug-design and elaboration of novel efficacious medications; forensic or medicinal chemistry; investigations for forensic medico-legal purposes; toxicology; nuclear forensics; pharmacy; agricultural and food science and technology; archaeology; geology; and more [10]. Mass spectrometry is implemented in the study of reactions of ozonation of pharmaceuticals for purposes of quality control and assessment of risk for human health and the environment due to pollution [11].

Despite superior instrumental performances of the analytical mass spectrometry, there is often a gap in transforming variables m/z and intensity of mass spectrometry (MS) peak to molecular structural knowledge [12]. There is an analytical challenge in distinguishing background signals or noise from the analyte ones. This fact prevents a reliable analysis of chemical reactions, thus highlighting the importance of ozonation. A reliable annotation of all measured analytes is a challenge in both quantitative and structural mass spectrometry, having, however, a significant effect on kinetics, thermodynamics, and diffusion parameters obtained mass spectrometrically. The chemical analysis is further complicated due to the structural diversity of interacting analytes, intermediates, and, frequently, products of interactions; the dynamic range of analytes and a lack of commercial internal standards, respectively. In addition, there are typically formed adducts of analytes that cannot be predicted a priori. The same is true for *fluctuations* of MS measurands. Due to these reasons, there are often

thousands of analyte signals that remain non-identifiable during mass spectrometric-based both quantitative and structural analyses.

Therefore, to derive from MS phenomena in combination with exact model equations reliable values for measurands and geometry parameters of species is of crucial importance for elaborating kinetic equations of AOPs. There lies a question: Do exact quantitative and structural data on chemical reactions and interacting molecular species, as well as the kinetics of processes, completely derive from MS experiments? It is answered in the affirmative by innovative model Equations (1) and (2) within the stochastic dynamics concept [13–26]. It overcomes the aforementioned drawback of methods for data-processing of MS variables, thus producing exact performances. For instance, studying the kinetics of triadimenol and sucralose in environmental samples via Equation (2), there is |r| = 1 [20]. The predictive capability of the formulas allows for making reliable assumptions about molecular structure and quantities of species depending on MS variables during chemical reactions. There are derived dynamical molecular properties from various spans of scan time and experimental factors. There is a crucial advantage of the innovative tool due to the fact that the developed, so far, methods for processing MS measurable variables exclude from processing the low-abundance MS signals of noise. An additional understanding of MS phenomena, depending on experimental conditions of measurements; thus, underlying collision energy or temperature is also provided by Equation (2) and its further deriving formulas. Despite excellent performances of these models, they have been tested on a small number of molecules. Due to this reason, this study adopts the very straightforward approach based on Equation (2), because it is empirically justified as an exact model for both the quantitative and 3D structural analyses among a set of ionization methods and a statistically representative number of molecules. Furthermore, it is tested on complex environmental samples, commercial products of multi-component mixtures, and biological fluids. The 3D structural analysis is performed when Equation (2) is used complementarily to Arrhenius' Equation (3).

$$D_{SD}^{tot} = \sum_{i}^{n} D_{SD}^{i} = \sum_{i}^{n} \left(1.3194 \times 10^{-17} \cdot A^{i} \cdot \frac{\overline{I_i^2} - \left(\overline{I}_i\right)^2}{\left(I_i - \overline{I}_i\right)^2} \right) \tag{1}$$

$$D_{SD}^{",tot} = \sum_{i}^{n} D_{SD}^{",i} = \sum_{i}^{n} \left(2.6388 \times 10^{-17} \times \left(\overline{I_i^2} - \left(\overline{I}_i\right)^2 \right) \right) \tag{2}$$

$$D_{QC} = \left[\frac{\prod_{i=1}^{3N} \nu_i^{(0)}}{\prod_{i=1}^{3N-1} \nu_i^{(s)}} \right] \times e^{-\frac{\Delta H^{\#}}{R \times T}} \tag{3}$$

The advantage of the innovative tool is crucial for processing mass spectra of AOPs of pharmaceutics due to the fact that the ozonation reaction involves various ion-radicals. A diverse number of intermediates and products. Moreover, the ozonation reaction lacks selectivity. This fact further challenges precise MS assignment and quantification of analytes via traditional approaches to MS data-processing. The species are not only at very low analyte concentrations, but also show low intensity of MS peaks. The strength of Equations (1) and (2) lies in the capability of exact processing of experimental MS noise and spatial-temporal fluctuations of measurands [11–25]. Both the reaction processes in bulk and in the gas-solution interphase are tackled exactly within the same model, Equation (2). It is applied to various ionization MS approaches.

In line with these innovations, this study first deals with quantitative and 3D molecular structural analysis of ozonation processes of pharmaceutics using Equation (2). The novel analytical data not only make a significant contribution to fundamental science, but also provide a prospective industrial scale implementation into developing effective WWPPs for wastewater clean-up technology.

The major motivation behind the choice of studied analytes is that nitroimidazole antibiotics are among the most widely used drugs for treating various diseases. These compounds typically remain unaltered through conventional WWPPs [1]. Thus, metronidazole is a common medication in urban and medical wastewater [1,2]. The MTZ exhibits high water solubility and low biodegradability; thus, significantly challenging its removal from sewage wastewater during WWPP reactions. Thus, MTZ has been found in water at concentrations within ng·dm^{-3} to mg·dm^{-3}. Employment in MS methods for studying solar photoelectron-Fenton reactions of MTZ has been illustrated [2]. MTZ has been employed as a model pharmaceutical in evaluating reactions of (photolytic) ozonation, as well [1–3]. However, the elaborated, so far, models have shown accuracy r^2 = 0.997–0.998 [2,6,20].

In ozone-based AOPs, hydroxyl radicals are the primary short-lived oxidizing species [1]. The MTZ exhibits a longer degradation time at about 30 min in order to achieve 100% effectiveness of the reaction. At pH > 8, there

is interaction of •OH radical generated via indirect ozonation with MTZ [6]. Its degradation reaction in the absence of UV-irradiation is [26]:

$$MTZ + 42\ (^{\bullet}OH) \rightarrow 6CO_2 + 24H_2O + 3NO_3^- + 3H^+ \quad (4)$$

2. Experimental

2.1. Materials and Methods

Mass spectrometric measurements have been performed via LTQ Orbitrap XL (Thermo Fisher Inc., Rockville, MD, USA) equipped with an ESI 2 source (Table S1). The quantification has involved a combination of mass detectors (trap, linear ion trap, and Orbitrap), accumulating spectra for t = 0–13 min; mass range *m*/*z* 200–2000; and resolution 70,000. Full scan and selected reaction monitoring methods. There are individual files. The chromatographic separation has been performed via a C18 column (4.6 mm × 150 mm, 5 mm) by isocratic elution with 30% CH_3CN and 70% ultra-pure H_2O (containing 0.1% HCOOH).

The sample preparation approach involves mixtures of pharmaceutics (99% purity), humic acid, and sodium hypochlorite solution (at about 13% chlorine concentration) (Sigma–Aldrich, Merck KGaA, Darmstadt, Germany). The solvents have been obtained from Sigma–Aldrich, as well. The same is valid for chemicals $KMnO_4$, $Na_2S_2O_3$, H_2O_2, H_2CO_3, and $NaHSO_3$, respectively. They have been used without further purification. Ozone was generated by an ozone generator with pure oxygen as the gas source.

Oxidants of ozone and permanganate, without or in the presence of H_2CO_3 have been studied due to oxidative degradation of pharmaceutics. A standard experimental design. The oxidation experiments have been performed in a 50–250 mL flask at T = 20–25 °C. For experiments with chlorine, permanganate, and H_2CO_3, the pharmaceutics were added in solution in order to obtain the designed initial concentrations (1 mg·L^{-1}). The 2 mg·L^{-1} of inorganics have been added separately. The ozonation involves: The ozone has been bubbled into the studied solution, thus achieving a concentration of 2 mg·L^{-1}; then, 1 mg·L^{-1} of pharmaceutics has been dosed. The reaction solutions have been continuously mixed using a magnetic stirrer. Between 10 and 25 mL of them have been treated with $NaHSO_3$ to remove chlorine and permanganate. In addition, $Na_2S_2O_3$ has been added to eliminate ozone. The quenched samples have been filtered by a 0.45 mm membrane. They have been separated via high-performance liquid chromatography for MS-based quantification and structural analysis of residual forms of medications.

The quantitative and 3D structural analyses of the discussed medications are verified using standard sample sets of MS data taken from works [13,14].

There have been used high resolution TSQ 7000 and Thermo Finnigan Surveyor HPLC system, having Surveyor MS-Pump, Surveyor Auto Sampler-Plus (injection volume: 0–20 mL) as well as Surveyor-Plus PDA detector (Thermo Fisher Inc., Rockville, MD, USA). A triple quadrupole mass spectrometer (TSQ 7000 Thermo Electron, Dreieich, Germany) equipped with an ESI 2 source has been used. Standard LTQ Orbitrap XL (Thermo Fisher Inc., Waltham, Massachusetts, USA) has been utilized. Chromatographic data were collected with a Gynkotek (Germering, Germany) HPLC instrument, equipped with a preparative Kromasil 100 C18 column (250 × 20 mm, 7 µm; Eka Chemicals, Bohus, Sweden) and a UV detector set at 250 nm. Separation of analytes has been carried out on a Synergi Polar (150 mm × 3 mm, 4mm particle size) from Phenomenex (Torrance, CA, USA), as well. The mobile phase consists of H_2O containing 1 mM $CH_3COO^-{\cdot}NH_4^+$ and 0.1% HCOOH (A) and CH_3CN containing 0.1% HCOOH (B). Samples have been processed using a flow rate of 500 mL.min^{-1} and a gradient program as follows: 100% solution A isocratic for 5 min; linear gradient to 60% of solution A for 10 min, and to 100% of solution B for 2 min. After 100% solution B isocratic for 6 min, the instrumentation system returned to its initial conditions (100% solution A) within a duration of 1 min. It has been held for a duration of 7 min before the next experimental run. MS detection has been carried out by a TSQ Quantum Ultra AM device (Thermo Scientific, Waltham, MA, USA) equipped with an ionization source operating in positive polarity. Nitrogen gas has been used as both the sheath (54.99 arbitrary units) and auxiliary (2.00 arbitrary units) flow gas. Argon gas served as the collision gas with a pressure of 1.1 mTorr. The capillary temperature for MS TSQ analysis has been 283.02 °C. The vaporizer T has been –63.17 °C. Tandem MS parameters have been optimized in conditions of continuous flow mode via injecting 1 ng·mL^{-1} of standard analyte solution. In addition to chromatographic retention time, the transitions of the most abundant and characteristic fragment product ions of analyte precursor ions have been monitored in SRM mode. Therefore, both the full scan and SRM spectra in this work.

High resolution MS spectra have been produced by means of an LTQ-Orbitrap Spectrometer (Thermo Fisher, Waltham, MA, USA), operating in positive polarity and mass range: 50–300. Automatic gain control has been used, thus providing high-accuracy MS measurements. The deviation is ≤2 ppm. The elemental composition has been determined by an internal calibration standard. The mass spectrometric equipment has an Agilent 1200 HPLC

system (Taufkirchen, Germany) containing an LC-Pump and a DAD detector. The auto sampler has been used injection volume of 10 mL. The same experimental conditions of separation of samples as described above for LC–MS/MS analyses. The tandem mass spectra were obtained by the CID fragment technique with a series of collision energy values discussed in the next sections. This study verifies both the single and tandem operation modes [27].

The ozonation control experiments have been carried out without quenching agents at various temperatures and pH values. The quenching experiments have been carried out as control experiments. The quenching agent, however, has been spiked into the ozonated solution at about 5 min toward selected target analyte has achieved 0.5–1.0 $mg \cdot L^{-1}$ concentration levels. The quenching agent volume spiked into the reacting solution has been determined based on reaction stoichiometry at about 25% of the expected quantity of the O_3 residual. The time point is obtained via the control test. The quenching agent volume has been at about 0.5% of the total reactor concentration control level of ozone. It depends on the quenching approach and reactor procedures. Commonly, the agent volume does not exhibit a measurable effect of dilution on ozone residual. The theoretical quenching completion time was determined using MS-based kinetic modeling, relying on intensity data from analyte peaks acquired over short scan-time intervals. It has been used that within the radical quenching analysis, the hydroxyl radical ($HO^{\bullet}$) is the major oxidative species as has been highlighted via reaction (4), above. It is obtained via reaction (5).

$$O_3^{-\bullet} + H_3O^+ \rightarrow HO^{\bullet} + O_2 \quad (5)$$

The radical-anion ($O_3^{-\bullet}$) is derived via reaction (3), while the anion (O_2^-) is derived via reaction (4).

$$O_3 + O_2^{-\bullet} \rightarrow O_3^{-\bullet} + O_2 \quad (6)$$

$$H_2O_2 \rightarrow O_2^{-\bullet} + H_3O^+ \quad (7)$$

The hydroxyl radical ($HO^{\bullet}$) is responsible for the degradation of MTZ, accounting for the degradation rate efficiency at 85%. Within this model, there is an MTZ concentration of 35.15 $mg \cdot L^{-1}$ and an ozone concentration of 0.837 $mg \cdot L^{-1}$. The experimental time is 0–13 min. There is used linear kinetics model $[c_{MTZ}]_{t1}/[c_{MTZ}]_{t0} = f(t)$ or $y = A + Bx$ ($A = -8.82589 \times 10^{11} \pm 2.86338 \times 10^{11}$; $B = 2.16463 \times 10^9 \pm 3.968 \times 10^8$; $|r| = 0.98361$; $sd(yEr\pm) = 3.367 \times 10^8$; $N = 3$, $p = 0.1154$). Files 22090921_H2O_i_pos.raw (i = 1–4) (Figure S4). The linear kinetic model uses average intensity [arb.units] data on MS peak at *m*/*z* $154.9078_5 \pm 1.72074.10^{-4}$ as followings: 8195.64985 (22090921_H2O_2_pos.raw); 5598.09653 (22090921_H2O_3_pos.raw); and 8195.64985 (22090921_H2O_3_pos.raw).

The analysis of SMX also involves correlation with the standard NIST spectrum as follows [https://webbook.nist.gov/cgi/cbook.cgi?ID=C723466&Mask=200#Mass-Spec, accessed on 26 June 2025].

2.2. Theory/Calculations

2.2.1. Stochastic Dynamics Mass Spectrometric Approach

The innovative stochastic dynamics mass spectrometric tool utilizes model Equations (1) and (2) as empirically proven MS laws obeyed by a set of soft-ionization MS approaches. Equation (2) is derived from Equation (1) (consider details on [13–25]). The 'I' denotes experimental MS intensity of the i^{th} peak. The A^i represents a statistical parameter obtained via SineSqr fitting of the functionality of the temporal distribution of intensity toward a span of scan time (t) or function $(I-\langle I\rangle)^2 = f(t)$. The *m*/*z* and intensity parameters on i^{th} analyte ion are described as random variables. The method is based on the modified Box–Müller method for generating random numbers. There is variation around $|r| = 1$ of SineSqr fitting of producing "A^i" data on Equation (1). It is simplified to Equation (2) approximating $A \equiv 2 \langle(I-\langle I\rangle)^2\rangle$.

Formula (2) overcomes the difficulty of traditional MS methods for processing of measurands, which face the determination of analytes in condensed phases. An exact quantitative analysis ($|r| = 1$) of analytes is produced. The formulas attempt to get behind current knowledge of MS phenomena. They tell us the ultimate truth about not only analyte concentration, but also its 3D molecular structure. Because empirical proof provided so far shows that the equations are capable of analysing the analyte quantity and its 3D molecular structure. The latter task, as aforementioned, is carried out when Equations (1) or (2) are used complementarily to Equation (3). The achieved, so far, superior *chemometrics* performances, particularly highlighting formula (2), show that Equation (2) quantifies precisely *fluctuations* of variables *pro* short span of scan time. The chemometric assessment of relation $D''_{SD} = f(D_{QC})$ of parameters of Equations (2) and (3) shows $|r| = 0.9999_4$, studying enantiomers of triadimenol in environmental samples [21]. The analysis of guanosines and flavonoids produces $|r| = 1$ [19]. The same is valid to

structural analysis of MTZ in biological fluids [14]. A review-article [16] details the application of Equation (1) to 3D structural analysis.

The D_{QC} parameter accounts for the energy value of 3D molecular conformation, electronic effects, and isotopologies of a molecular object. Chemometric assessment of relation $D''_{SD} = f(D_{QC})$ allows us not only to determine exactly 3D molecular structures of enantiomers, but also molecular isotopologies.

Both the theoretical and experimental designs are governed by seeking connections between experimental MS phenomena and the 3D molecular structure of analytes. There are accounted for that the developed methods for processing variables frequently show semi-quantitative data. The highlights are on analytes in low concentrations of multi-component samples. Only approaches yielding exact quantitative data have fundamental importance for multidisciplinary fields of research implementing mass spectrometry. Because there is a key question of how to determine quantities much more accurately, thus allowing for the differentiation of reliably observable MS peaks of species among various 3D molecular and electronic structures of analytes. The latter task is of crucial importance for the development of reliable and effective clean-up technologies as well as programmers for monitoring and assessing the risk for both human health and the environment from xenobiotics. Herein, there is reflected in mind analysis of pharmaceutics and their products of chemical interactions with ozone.

2.2.2. Quantum Chemical Computations

The theoretical analysis was carried out by GAUSSIAN 98, 09; Dalton2011, and Gamess–US program packages [28–30]. The thermochemical parameters were obtained using geometry optimization of the studied species by ab initio and DFT methods. The Becke 3-parameter exchange with Lee–Yang–Parr correlation, Becke 3-parameter Perdew–Wang–1991, w-B97X–D, QCISD, and long–range corrected–PBE (Perdew-Burke-Ernzerhof) as well as Truhlar's M06, M06–2X, and M06–HF functionals were used [31–35]. The Bernys' algorithm was utilized for GS computations. The stationary points on potential energy hypersurfaces were obtained using standard analytical harmonic vibration analysis. The absence of imaginary frequency has confirmed the minima. Rotational constants were extracted from optimized geometries. When used in internal energy determinations via Rice–Ramsperger–Kassel–Marcus calculations, the frequencies were scaled by 0.99. The Dunning's basis sets (cc-pVnZ) (n = D, T, and 5), 6–31++G(2d,2p), and quasirelativistic effective core pseudo potentials from Stuttgart–Dresden(–Bonn) (SDD, SDDAll, http://www.cup.uni-muenchen.de/oc/zipse/los-alamos-national-laboratory-lanl-ecps.html, accessed on 22 October 2025) were used. The MM2/MD computations of interacting molecular ensembles have also been carried out. Molecular mechanics calculations were performed, using DREIDING and UFF force fields. The theoretical analysis obtains electrostatic potentials and natural bond orbital charges; thus, assessing the protonation capability of the species, as well [36,37]. The Allinger's molecular mechanics force field MM2 was utilized [38,39]. The low-order torsion terms are accounted for with higher priority rather than van der Waals interactions. The accuracy of the method compared with experiment is 1.5 $kJ \cdot mol^{-1}$ of diamante [38] or 5.71×10^{-4} a.u.

The MD computations were performed by ab initio and DFT BOMD. It was carried out at M062X functional and SDD or cc-pvDZ basis sets, as well as without considering the periodic boundary condition. The trajectories were integrated using a Hessian-based predictor-corrector approach with Hessian updating for each step on BO-PES. The step sizes were 0.3 and 0.25 $amu^{1/2}$ Bohr. The trajectory analysis stops when: (a) centres of mass of a dissociating fragment are different at 15 Bohr, or (b) when the number of steps exceeds the given input parameter maximal number of points. The total energy was conserved during the computations within at least 0.1 $kcal \cdot mol^{-1}$. The computations were performed by means of fixed trajectory time speed (t = 0.025 fs) starting from initial velocities. The velocity Verlet and Bulirsch-Stoer integration approaches were used.

2.2.3. Chemometrics

The software R4Cal Open Office Statistics for Windows 7 was used. The statistical significance was checked by a *t*-test. The model fit was determined by the F-test. The ANOVA tests were also used. The nonlinear fitting of experimental MS data was carried out by means of a searching method based on the Levenberg-Marquardt algorithm [Apache OpenOffice, [http://de.openoffice.org]] [40]. ProteoWizard 3.0.11565.0 (2017), mMass 5.5.0, and AMDIS 2.71 (2012) software were utilized.

3. Results

3.1. Mass Spectrometric Data—Fragmentation Pattern

An assignment of analytes is performed in the studied samples of ozone depletion. The metabolomics show *m*/*z* 254.05939 (sulfamethoxazole), 237.10224 (carbamazepine), and *m*/*z* 172.07167 (metronidazol) [27]. However, oxidation processes of dissolved organic carbon and SMX data show a similar MS pattern with MTZ. There are revealed peaks at *m*/*z* 235.53, 190.17, 187.97, 176.11, 160.30, and 155.93 [41]. The fragment paths of SMX are detailed in [14]. Thus, the analysis herein involves a comparative study of fragment paths of all analytes.

Furthermore, heterocyclic intermediates and OH-derivatives obtained due to solar photoelectron-Fenton reactions of MTZ have been [2] obtained via MS methods at pH 3.0 in the solar flow plant. The MTZ exhibits MS peaks at *m*/*z* 218, 202, 186, and 170, while 3-(2-hydroxy-ethyl)-2-methyl-3H-imidazol-4-ol shows peaks at *m*/*z* 189, 173, 157, and 141, respectively [2]. The 2-methyl-5-nitro-1H-imidazole and 2-methyl-3H-imidazol-4-ol reveal peaks at *m*/*z* 126 and 97. Despite experimental conditions, there is a pharmacokinetic interaction with •OH radical. Thus, the study, herein, involves mechanistic aspects of MTZ processes of •OH radical. The interaction scheme (Figure 1) attempts to explain the observable MS data on Figure 2. The proposed radical-cations agree with low intensity values of peaks, which are frequently found in MS spectra of radicals.

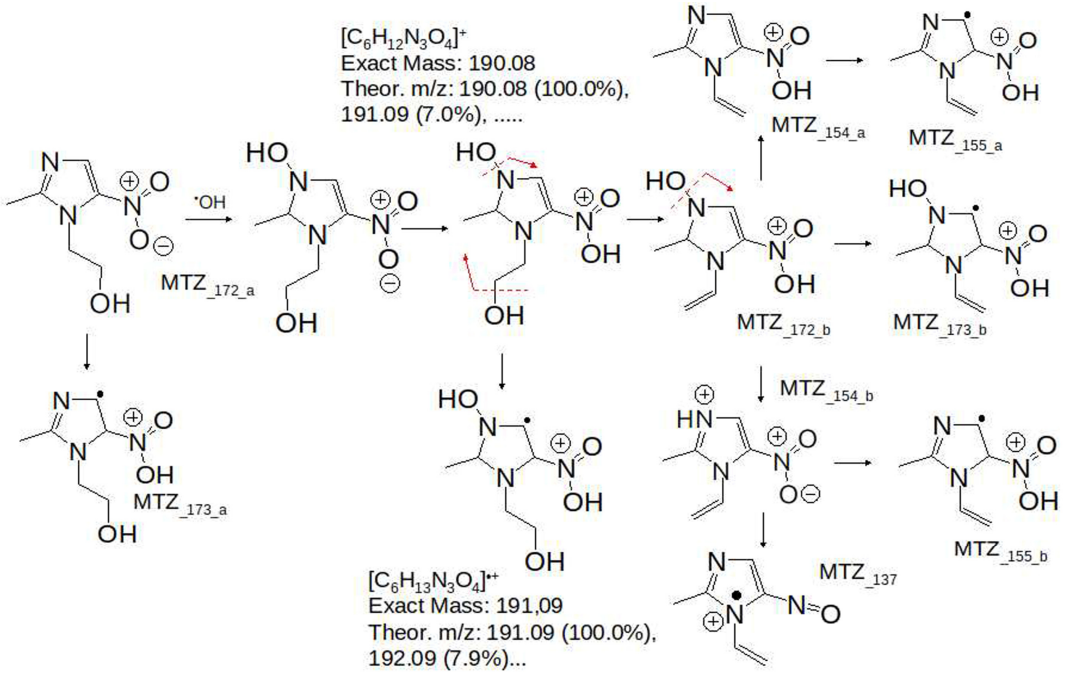

Figure 1. Interaction scheme of metronidazole with •OH radical generated via ozonation; theoretical exact mass, *m*/*z* values, and relative intensity ratios [%] of the isotope peaks.

On the other hand, caffeoylquinic acid metabolites are obtained due to phenylpropanoid biosynthesis. They play a defensive role against stress in plants. Conversely, in humans, CQAs exhibit therapeutic effects [42]. The presence of CQAs in environmental samples could be attributed to plants and dietary to humans. Due to interactions with carbonyl compounds or radicals of H_2CO_3, depending on the pH of the environmental sample, there are chemically substituted products of interactions, as well. Carbonyl compounds as, for instance, formaldehyde are highlighted as common oxygenated by-products of ozone. They are considered environmental aquatic pollutants due to adverse health effects [43–45]. The same is true for the discussed processes in dissolved organic matter. Ozonation produces aldehydes, ketones, and carboxylic acids [46–48]. The cycloaddition reaction with ozone yields cyclic products as well [47]. In the presence of H_2CO_3 there are also products of $•CO_3^-$ anion-radical [48] and $•HCO_3$ radical [49]. They cause novel substituted 3-, 4- or 5-carboxyoxy-1,3,5-trihydroxy-cyclohexanecarboxylic acids via interaction with QA (Figure 3). Figure 3 depicts a competitive compound producing a set of common MS peaks as aforementioned MTZ derivatives.

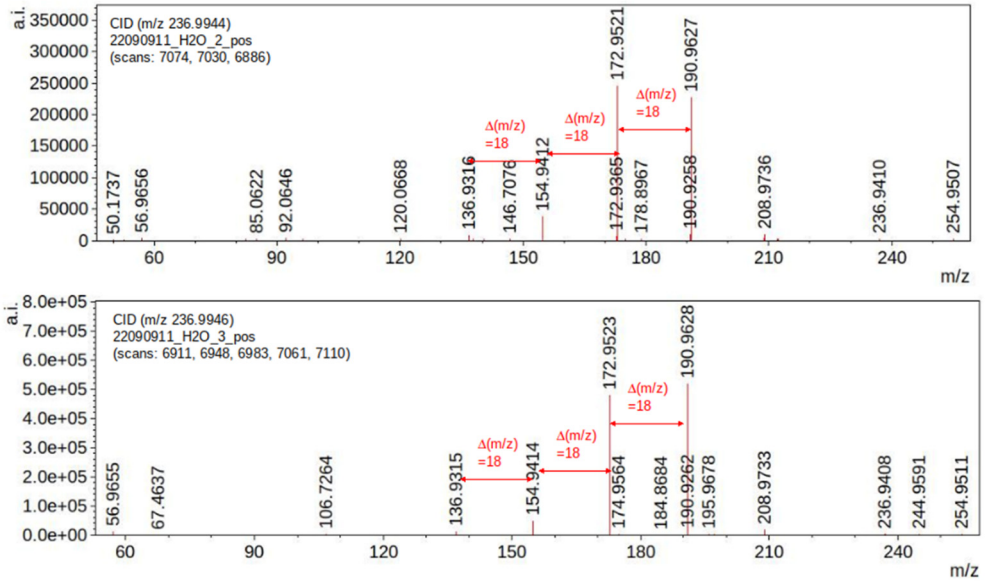

Figure 2. Experimental collision-induced dissociation mass spectra of ions at *m/z* 236.9944 and 236.9946 of samples 22090901_H2O_2_pos and 22090901_H2O_3_pos, depending on the retention time or scan number (continued as Figures S1–S3).

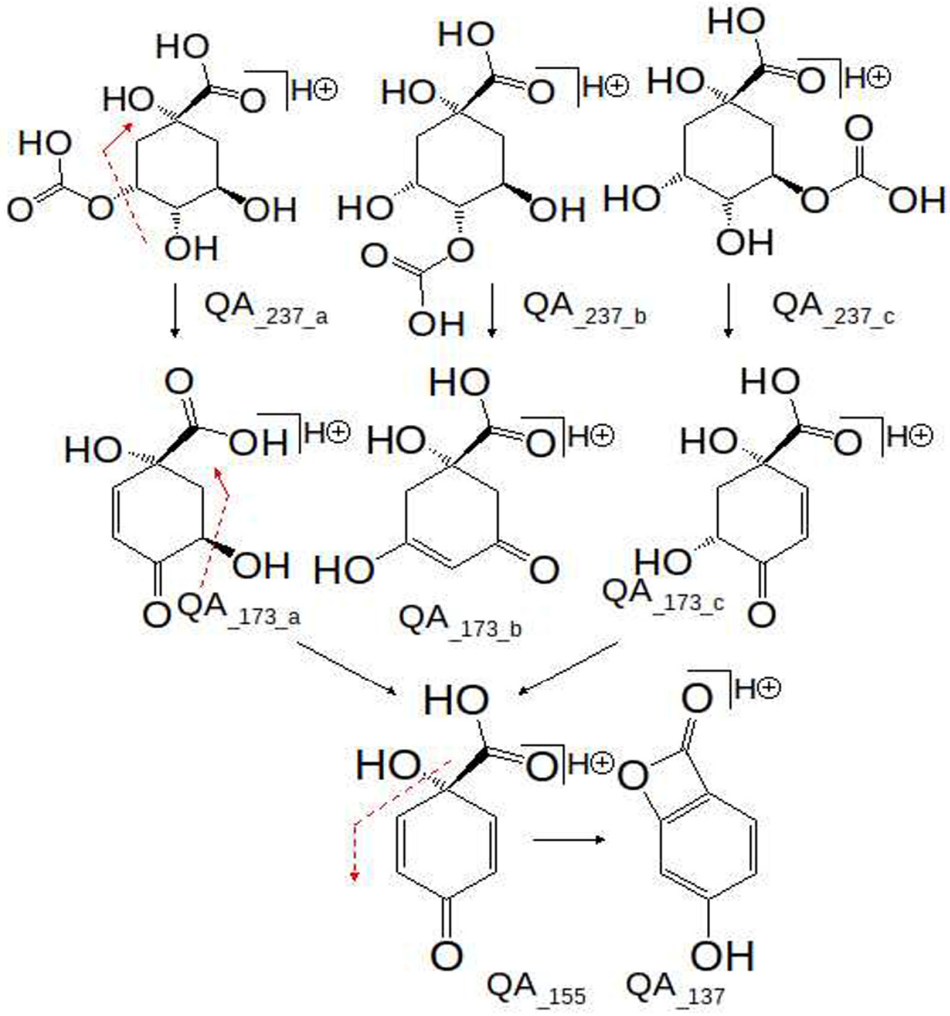

Figure 3. Chemical diagrams of proposed fragment species of substituted quinic acid species obtained via interactions with $^{\bullet}CO_3^-$ anion-radical and $^{\bullet}HCO_3$ radical, and, depending on the proton-accepting capability of the ions and their tautomers.

Further: The so-called tingle analytes belong to the alkenamide family of organics. They have been extensively examined due to their sensorial effect. It is perceived on teeth, gums, the roof of the mouth, and more [50]. The analytes are of particular interest in organic synthesis and catalysis, as well [51]. Herein, it should be emphasised that the discussed analytes exhibit MS spectra showing an abundance peak at *m*/*z* 98–102 (relative intensity 100%) and a low abundance one within *m*/*z* 110–119 (55–73%) depending on the type of substituents.

Looking at the experimental spectrum depicted in Figure 4 [29], it could be assumed to be an alkenamide derivative. It is assigned precisely via Equations (2) and (3) (below).

The proposed analytes are a response to the dominant problem of experimental MS assignment of *fluctuations* of low-abundance peaks. Figure 4, in the latter context, details it. The spectra of scan numbers 4974 and 7061 of sample 220090902_Kali_Pu_Penc_2.0HCO3_0_pos show low abundance peaks at *m*/*z* 172 and 191, as well as intensive ones at *m*/*z* 99 and 116. This fact makes a reliable analyte assignment.

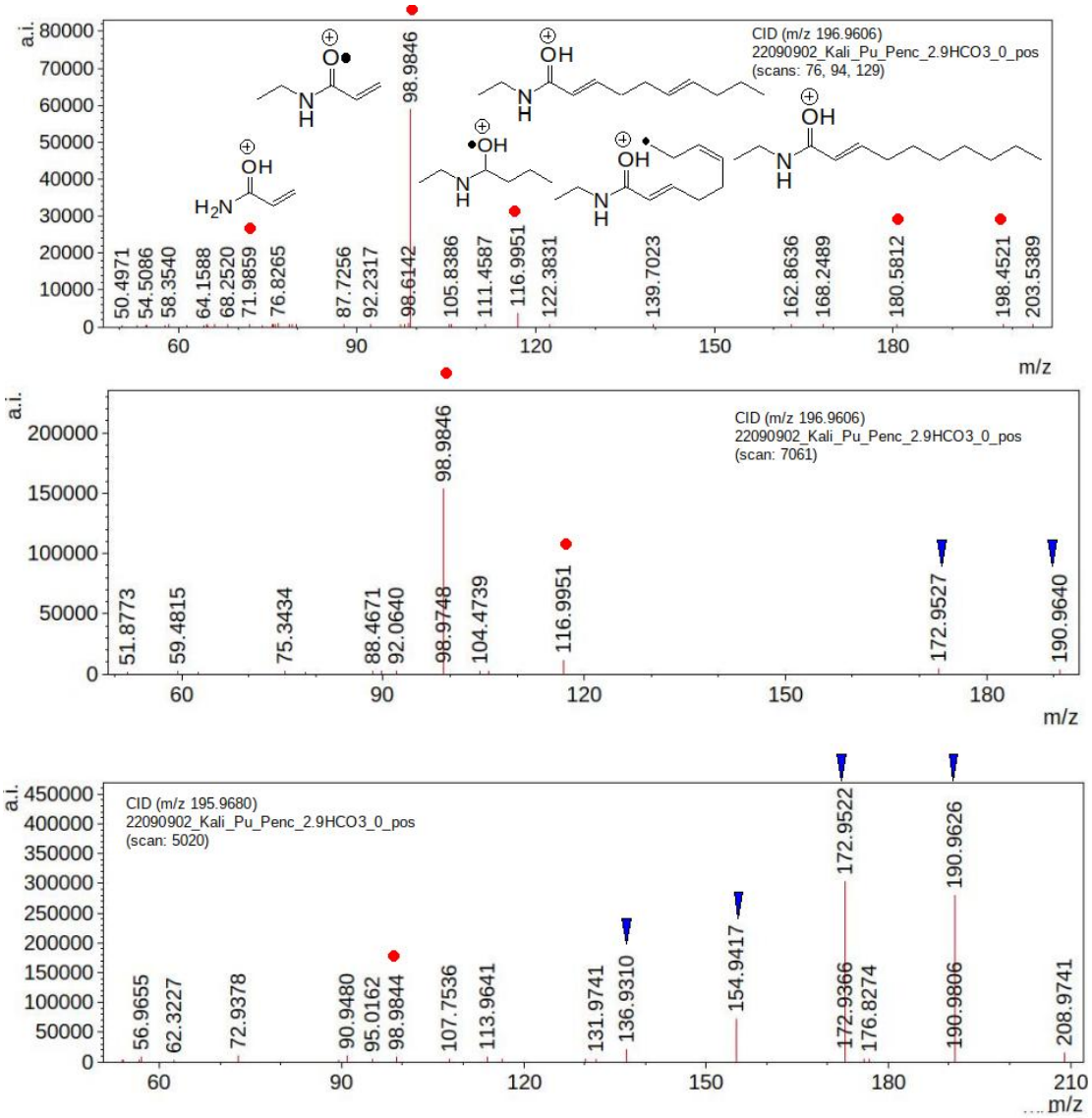

Figure 4. Experimental collision-induced tandem mass spectra of ions at *m*/*z* 196.9606 and 195.9680 of sample 22090902_Kali_Pu_Penc_2.9HCO3_0_pos, depending on retention time or scan number.

Conversely, data on scan 4948 (Figure 2) of sample 22090911_H2O_2 show the same abundance peaks at *m*/*z* 137, 155, 173, and 191, while results from scans 76, 94, and 129 show abundance peaks at 99, 106, and 117.

Therefore, there should be addressed: Could low abundance peaks at *m*/*z* 172 and 191 of the MS spectrum of scan numbers 4974 and 7061 be assigned to the same species of sample 22090911_H2O_2 illustrated in Figure 2? This question remains unanswered due to scarce empirical research on the assignment of noise and fluctuation of low-abundance MS variables. The algorithms for automated data-processing of measurands do not detail fluctuations of variables.

However, the stochastic dynamics model Equation (2) is the first method allowing for exact processing of all observed peaks and their precise assignment to 3D molecular structures of analyte ions, when it is used in Equation (3). The issue is of crucial importance for MS methods using direct analysis. As work [14] reports, there is an exact assignment of MTZ ions in biological fluids using Equation (2).

Empirical proof that this could be so in this study comes from the following sub-sections dealing with quantitative and 3D structural analysis of observable species using Equations (2) and (3).

The MS spectra of scan 112 of sample 22090901_H2O_1_pos (Figure S4) are assigned to CBZ. Equations (2) and (3) have been successfully applied to reliably assign oxidized products of CBZ in marine dissolved organic matter [13]. This study chemically assigns observable data on [27] to the discussed analyte using a standard dataset of CBZ spectra measured in various conditions [13], which has been further proven by omics methods [27].

3.2. Mass Spectrometric Data—Quantitative Analysis

To begin with, let us try in this subsection to see how Equation (2) is applied to quantify analytes. There is highlighted its capability of improving method performances, selectivity, and sensitivity. Before we start, important data on the performances of MS quantification via traditional methods should be illustrated. Figure 5 shows the linear correlation between average intensity data on analyte MS peak and concentration, studying CID-MS/MS spectra of ions at m/z $236.941_0 \pm 4.25631 \times 10^{-4}$, m/z $190.95_7 \pm 0.01526$, m/z $172.949_{96} \pm 0.00585$, and $154.941_5 \pm 1.99904 \times 10^{-4}$, respectively. There is obtained $|r| = 0.9896_5$–0.99_{983}. Although in the case of peak at m/z 190.95644 ± 0.01526, $|r| = 0.99_{983}$, it should be underlined that the analysis involves relatively short spans of scan time and measurands are considered as objects of equality on the base on chemometrics. There is projected data on a numerical scale as equal due to ANOVA parameters (Table S2). However, there is a significant standard deviation. It alters performances of the traditional method.

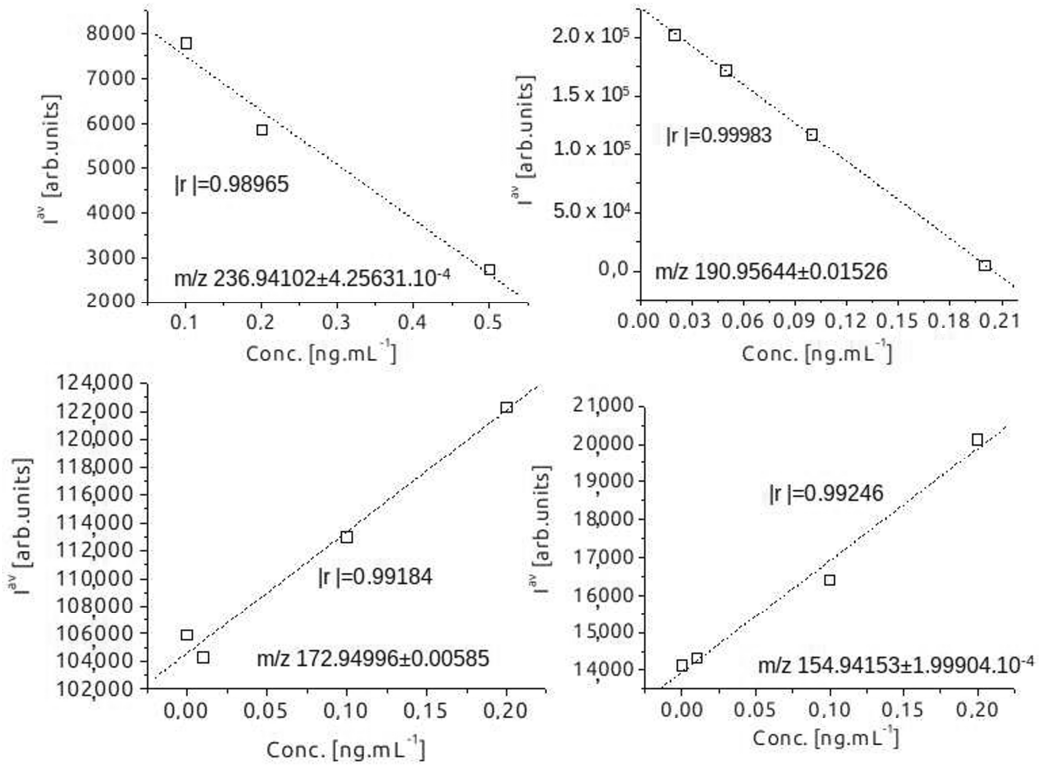

Figure 5. Linear correlation between average intensity data on short spans of scan time (Table S3) of CID-MS/MS peaks at m/z $236.941_0 \pm 4.25631 \times 10^{-4}$, m/z $190.95_7 \pm 0.01526$; m/z $172.949_{96} \pm 0.00585$; and $154.941_5 \pm 1.99904 \times 10^{-4}$ with respect to analyte concentration [ng·mL^{-1}]; chemometrics.

Looking at experimental data in Table S3, it should be further highlighted that the application of both the ANOVA and t-test to MS variables supposes their normal distribution. Thus, there is assessed consistency of experimental data sets. There is used the Shapiro– Wilk test. There are examined m/z-variables *per* short span of scan time, because Equation (2) processes MS measurable data *per* span of scan time of a measurement. It applies to collected MS variables over the entire time of a measurement, as well. The W-statistic provides the best power for assessing the normality of the distribution of variables [52–54] (Table S4). The tabulated data reveal that the studied sets of variables are normally

distributed. There are large W-values [52]. The latter test is not robust. It is utilized with a probability plot of datasets of variables, as well (Figure S5). When a plot lies from a line, then the measurands are normally distributed.

Conversely, when there is a deviation from linearity, the datasets could be outliers. The histogram and probability plots of results from the data in this study indicate that there is a point out of line. It is a peak at *m/z* 57. The data are illustrative, tackling the relation between physical laws, i.e., Equation (2), and laws of numbers or measurable variables, because behind Equation (2), there is a linear correlation between D''_{SD} parameters and parameters of Equation (3). This allows for fitting off MS measurands, for instance, the intensity of the peak of an ion with a 3D molecular structure. In other words, even though the relation between I^{av} of ion at *m/z* 57 toward concentration of analytes causes a relatively high $|r| = 0.99_{448}$ (Table S3), it can hardly be attributed to the reliable quantification of analyte. There is a possible contribution of the random error of measurement. Therefore, a high |r|-value as the only criterion, assuming reliable quantitative analysis, does not always indicate a reliable analysis. Because, behind any measured dataset of values, there is a real physical law determining the 3D and electronic structure of the analyte.

In carrying out MS measurements, there is reduced noise. However, it could never be eliminated. Furthermore, the temporal distribution of measurands could not be theoretically predicted. Thus, MS measures *per* any span of scan time should ultimately ascertain whether it fits within a certain value of another span of scan time to achieve exact data processing of experimental MS data. Due to fluctuations of measurands, there is a deviation from intensity data on species measured in multiplication and toward analyte concentration (Figure S6 and Table S5). The latter figure depicts an illustrative example of an ion at *m/z* 172.93663 of the CID-MS/MS spectra of a peak at *m/z* 236.9944 measured in multiplications. It is obtained using H2O_i_pos samples (i = 2–4) (Figures 2 and S1) showing deviation from absolute mean intensity value |r| = 0.6868–99456. So far, among developed MS methods, only Equation (2) is proven as an MS law valid for any span of scan time and provides exact data-processing of measurands. It processes any fluctuation of any variable within any span of scan time.

Therefore, in what follows in this sub-section, the capability of Equation (2) to overcome the drawback of traditional methods. An exact and reliable quantitative and structural analysis is produced.

Figures 6 and 7 detail the relation $D''_{SD} = f(\text{conc.})$ of parameters of Equation (2) instead of average intensity data on peaks (see Table S6, as well). There is a significant improvement in method performance. The best |r|-parameter among the studied ions is |r| = 0.99995 (*m/z* 154.94145 ± 7.07107 × 10^{-5}). A particular illustrative example of the advantages of Equation (2) is the analysis of CID-MS/MS spectra of an ion at *m/z* $136.931_2 \pm 2.828 \times 10^{-4}$, showing |r| = 0.57656 (Figure 7A). The traditional method of assessing relation $I^{av} = f(\text{conc.})$. Conversely, there is |r| = 0.99979 (Figure 7B) via innovative Equation (2) and chemometric assessment of relation $D''_{SD} = f(\text{conc.})$.

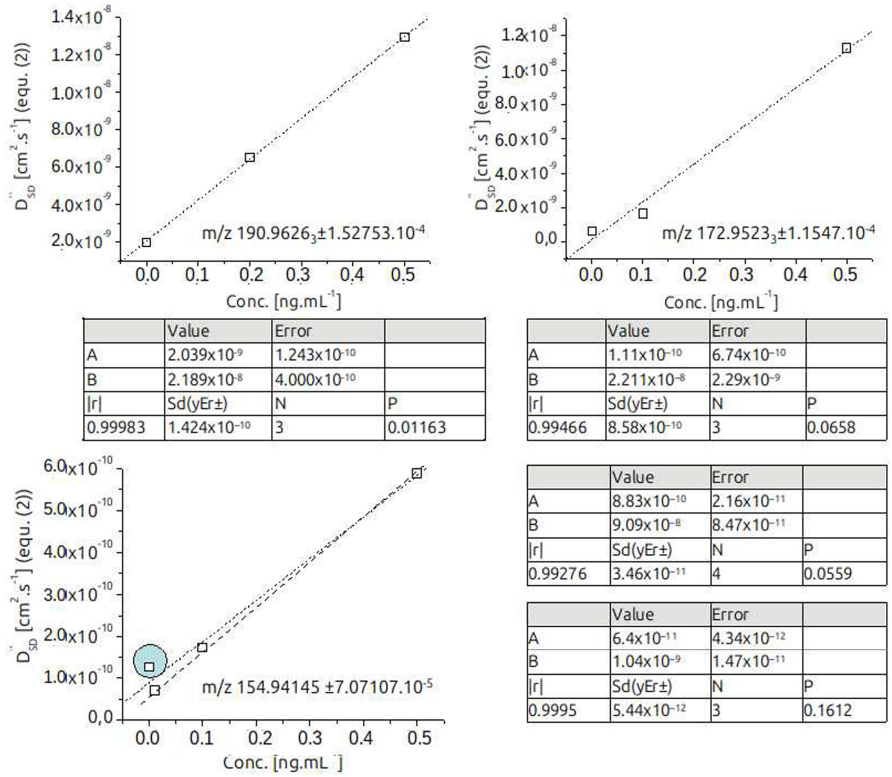

	Value	Error	
A	2.039x10^{-9}	1.243x10^{-10}	
B	2.189x10^{-8}	4.000x10^{-10}	
|r|	Sd(yEr±)	N	P
0.99983	1.424x10^{-10}	3	0.01163

	Value	Error	
A	1.11x10^{-10}	6.74x10^{-10}	
B	2.211x10^{-8}	2.29x10^{-9}	
|r|	Sd(yEr±)	N	P
0.99466	8.58x10^{-10}	3	0.0658

	Value	Error	
A	8.83x10^{-10}	2.16x10^{-11}	
B	9.09x10^{-8}	8.47x10^{-11}	
|r|	Sd(yEr±)	N	P
0.99276	3.46x10^{-11}	4	0.0559

	Value	Error	
A	6.4x10^{-11}	4.34x10^{-12}	
B	1.04x10^{-9}	1.47x10^{-11}	
|r|	Sd(yEr±)	N	P
0.9995	5.44x10^{-12}	3	0.1612

Figure 6. Functional relation between D''_{SD} data on Equation (2) versus analyte concentration [ng·mL^{-1}] of measurable variables of CID-MS/MS spectra of analytes as summarized in Table S6; chemometrics.

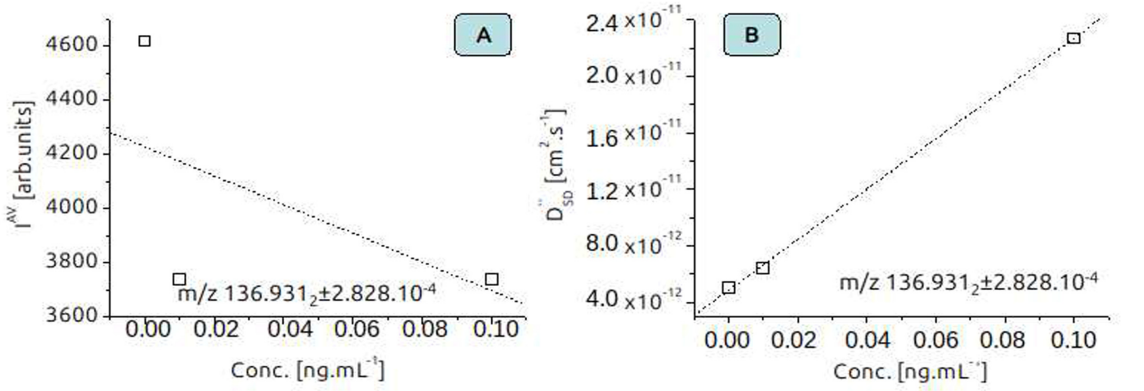

	Value	Error	
A	4227.0003	436.732	
B	–5311.349	7526.886	
|r|	Sd(yEr±)	N	P
0.57656	586.26016	3	0.6087

	Value	Error	
A	4.87×10^{-12}	2.12×10^{-13}	
B	1.78×10^{-8}	3.65×10^{-12}	
|r|	Sd(yEr±)	N	P
0.99979	2.8×10^{-13}	3	0.91221

Figure 7. Functional relations I^{av} = f(conc.) (**A**) and $D''_{SD} = f$(conc.) (**B**) of CID-MS/MS intensity data on ion at *m/z* 137 of samples 22090902_Kali_Pu_Penc_2.9HCO3_0_pos, 22090902_Kali_Pu_Penc_2.9HCO3_0.1_pos, and 22090902_Kali_Pu_Penc_2.9HCO3_0.01_pos at spans of scan time 6786–6986; 6846–7032; and 6912–7055 (Table S6); average intensity data I^{av} [arb.units] are from same spans of scan time and a set of samples with shown concentrations [ng·mL^{-1}]; chemometrics.

3.3. Mass Spectrometric Data—Structural Analysis

The test of the innovative Equation (2), so far, has empirically justified that macroscopic MS measured random variables and macroscopic (spatial)-temporal distribution of intensity data on MS peaks of analyte ions relate to microscopic properties and parameters of the molecule via the relation $D''_{SD} = f(D_{QC})$. The D_{QC} parameter of Equation (3) reflects free Gibbs energetics of species at GS and TS. There is a unique aspect to 3D molecular and electronic structures of species or to a 3D map of electron densities of atoms in a molecule. It is the value of the free Gibbs energy. The chemometric assessment of the latter relation links between MS measurands and analyte 3D and molecular structures. Because there are some unique molecular vibration models that are also implemented into Equation (3). It also accounts for vibration modes of species of both GS (n^i_o) and TS ($n^i_{(s)}$). The $DH^{\neq}$ reflects the activation enthalpy of the transition state. The R represents the universal gas constant. The change of vibration entropy accounts for the entropy contribution to the activation free Gibbs energy. The saddle point mode of imaginary frequency is excluded from calculations of D_{QC}-parameters [50].

Therefore, an accurate theoretical study of molecular species observable in certain MS conditions of measurement relates to macroscopic MS variables via the relation $D''_{SD} = f(D_{QC})$. Despite the complexity of the free Gibbs energy function, there are accurate approaches to determine it via DFT methods. This allows us to describe and predict the macroscopic distribution of measurands of molecular, respectively, ionic species toward their 3D molecular structures in the context of a 3D map of electron densities of atoms in these molecules or ions. This sub-section highlights the advantages of the complementary use of Equations (2) and (3) as well as DFT methods for computing accurate energetic and vibration modes of both the GS and TS of ions. In so doing, there are exactly quantified analytes as previously persuasively and empirically justified. However, Equation (2) is also used to simultaneously determine molecular structures of analytes.

In studying relation $D''_{SD} = f$(conc.) within concentration range 2.5 to 25,000 ng·mL^{-1} of spiked urine samples and fragment ions of MTZ at *m/z* 171.099_8, 172.071_8, 172.040_{81}, 213.146_3, 181.07_{22}, and 151.111_4, an exact performance |r| = 1 looking at data on *m/z* 172.0408_1 [14]. The developed protocol has been agreed with Commission Decision 2002/657/EC [55,56]. The confirmation criteria are: "(a) The relative retention time of an analyte (ratio retention time analyte to its internal standard) in a sample and a calibration solution had to be within the ±2.5% tolerance; (b) The presence of four identification points (parent ion and two daughter ions); and (c) The relative ion intensities had to comply with the permitted tolerances."

The marked method performances achieved via Equations (1) and (2) assume a drastic improvement of MS protocols. Moreover, the non-substituted MTZ is found in biological fluids. This fact raises an important issue about rethinking the applicability of Equation (2) as an alternative to becoming traditional quantitative protocols using total mass spectrometric intensity (I^{TOT}) [55]. Comparative study of MTZ according to Council Directive of

17.8.2002 (2002/657/EC) for high-resolution MS measurement standard within the traditional approach has led to |r| < 0.99 [14]. The same is valid for chemometric data on relation $D''_{SD} = f(D_{QC})$ of parameters of Equations (2) and (3) of MTZ in urine, showing a significant parameter |r| = 0.9814 in distinguishing tautomeric forms of the analyte. These results indicate that in biological fluids, MTZ stabilizes ions at *m*/*z* 171.099 of cation-radical $[MTZ]^{+\bullet}$, while peaks at *m*/*z* 171.072 and 172.041 correspond to its protomers. The peak at *m*/*z* 172.072 belongs to N^{3+}-cation, while the peak at *m*/*z* 172.041 is assigned to $N^{+}O$-cation. There is a lack of chemical substitution of MTZ in urine.

Conversely, the results from the current study clearly indicate that ozonation of MTZ causes its chemical substitution; thus, proposing a fragment scheme as depicted in Figure 1. The data on N^3–OH derivative agree with the previous study of the proton-accepting capability of MTZ. It shows that, depending on the pH value of the medium, there are formed $N^{3+}H$-cation [57] is formed. The same is true for its radical-cation species. The radical-cation formation frequently occurs for easily oxidizable compounds as MTZ. The proposed N^3–OH derivative of MTZ, herein, agrees well with theoretical data on proton affinity of a series of structurally very similar compounds. It is shown that M062x/6-311+G(d,p) ionic optimization of MTZ and ronidazole protonated at N^1-position converged into N^3-protomers [57]. The results from this study utilizing M062X/SDD level of theory produce the same result (Table S7); furthermore, various zwitterionic forms are accounted for.

Looking at excellent performances [14] of 3D structural analysis of species in complex samples via chemometric assessment of relation $D''_{SD} = f(D_{QC})$, the same model equations have been used, herein. The attempt is not only to assign reliably observed MS spectra of Figure 2, but also to determine their 3D structures. Within the fragmentation modes of substituted MTZ, there are obtained parameters of Equation (3); thus, computing GS and TS energetics and vibration modes of analyte protomers, tautomers, and cation-radicals (Table S7–S9 and Figure S7).

The reader's attention is focused on the major analytical challenge to distinguish MS background noise from the analyte peak belonging to a fragment ion in environmental samples [12]. In the case of MTZ, it focuses on the ion at *m*/*z* 97 (Figure S8). Looking at experimental data on samples 22090902_Kali_Pu_Penc_2.9HCO3_0.1_pos and 22090902_Kali_Pu_Penc_2.9HCO3_0_pos (Table 1), the correlative analysis between D''_{SD} data on ions at *m*/*z* 97, 137, and 155 shows |r| = 0.99997 (Figure 8). There are excellent performances. Despite the very low intensity of the former ion, it can hardly be associated with noise. There is a significant standard deviation of ion at *m*/*z* 97.1 ± 0.5 of the sample set Kali_Pu_Penc_2.9HCO3_0_pos. It alters overall method performance. As measurable variables from the latter table reveal, the analysis, herein, is based on intensity parameters of the discussed ions of two experimental conditions of measurements. Despite an excellent correlation being obtained between theoretical D_{QC} parameters of Equation (3) and experimental MS parameters of intensity data (absolute intensity data or D''_{SD} parameters of Equation (2)) on peaks (Table 1), thus, achieving |r| = 0.93957.

Table 1. measurable variables of a set of Kali_Pu_Penc_2.9HCO3_0_pos and _Pu_Penc_2.9HCO3_0.1_pos samples per span of scan time or scan number; *m*/*z* and absolute intensity (I [arb.units]) data on CID-MS/MS peaks; descriptive statistics; data on Equation (2).

22090908_Kali_Pu_Penc_2.9HCO3_0.1_pos						
Scan	***m*/*z***	**I**	***m*/*z***	**I**	***m*/*z***	**I**
5610	97.18535	2720.656	136.9318	5598.816	154.9414	20,652.12
7055	97.07042	2875.206	136.931	6164.307	154.9419	13,187.52
Mean	97.1_3	-	136.931_4	-	154.941_6	-
sd(yEr±)	0.08126	-	5.29×10^{-4}	-	3.56×10^{-4}	-
se(yEr±)	0.05746	-	3.74×10^{-4}	-	2.52×10^{-4}	-
<I>	-	2797.931	-	5881.561	-	16919.82
$<I>^2$	-	7.83×10^6	-	3.46×10^7	-	2.86×10^8
$<I^2>$	-	7.83×10^6	-	3.47×10^7	-	3.00×10^8
$<I^2>-<I>^2$	-	5979.126	-	80,005.62	-	1.39×10^7
D''_{SD}	-	1.58×10^{-13}	-	2.11×10^{-12}	-	3.68×10^{-10}
22090908_Kali_Pu_Penc_2.9HCO3_0_pos						
Scan	***m*/*z***	**I**	***m*/*z***	**I**	***m*/*z***	**I**
6438	97.46603	2896.065	136.931	3993.475	154.9418	23,072.7
6984	96.71831	3426.962	136.9317	4348.084	154.9413	16,284.14
Mean	$97._1$	-	136.931_4	-	154.941_6	-
sd(yEr±)	0.52871	-	$4.74.10^{-4}$	-	$3.22.10^{-4}$	-
se(yEr±)	0.37386	-	$3.35.10^{-4}$	-	$2.28.10^{-4}$	-
<I>	-	3161.513	-	4170.779	-	19,678.42
$<I>^2$	-	1.00×10^7	-	1.74×10^7	-	3.87×10^8
$<I^2>$	-	1.01×10^7	-	1.74×10^7	-	3.99×10^8
$<I^2>-<I>^2$	-	70,502.64	-	31,468.45	-	1.15×10^7
D''_{SD}	-	1.86×10^{-12}	-	8.30×10^{-13}	-	3.04×10^{-10}

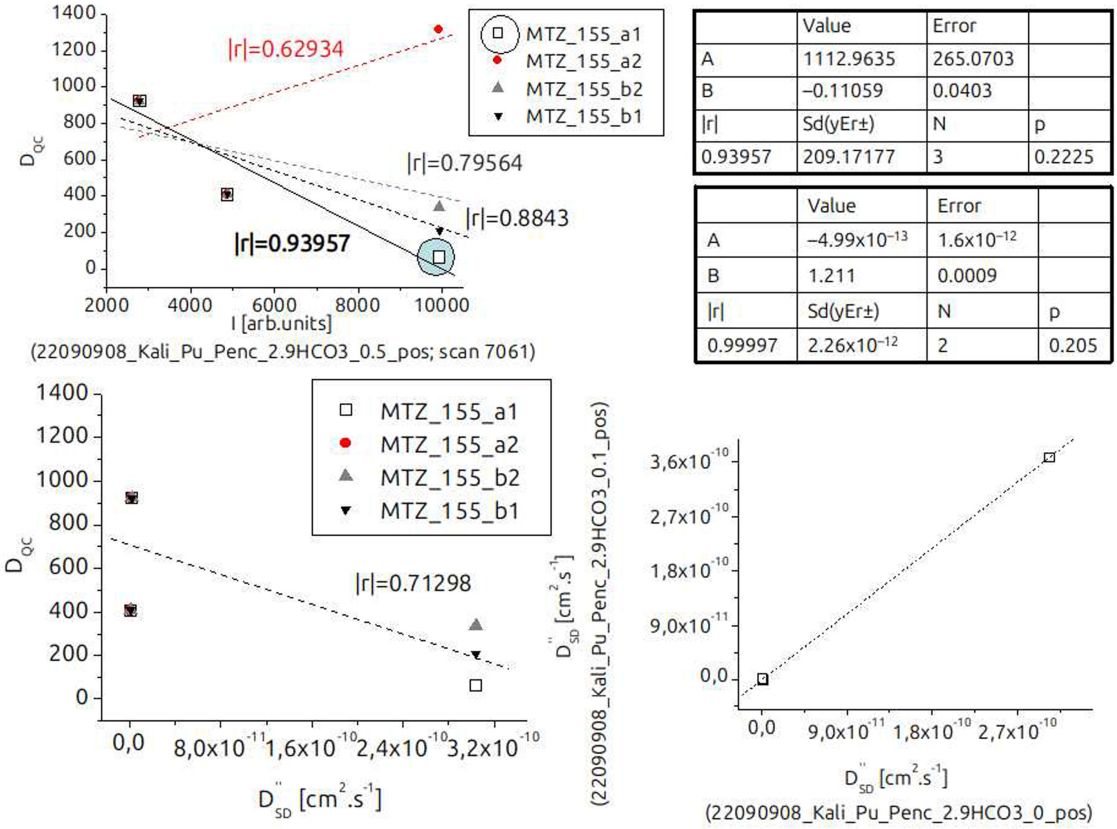

	Value	Error	
A	1112.9635	265.0703	
B	–0.11059	0.0403	
|r|	Sd(yEr±)	N	p
0.93957	209.17177	3	0.2225

	Value	Error	
A	-4.99×10^{-13}	1.6×10^{-12}	
B	1.211	0.0009	
|r|	Sd(yEr±)	N	p
0.99997	2.26×10^{-12}	2	0.205

Figure 8. Correlative analysis of $D''_{SD} = f(D_{QC})$ and $I = f(D_{QC})$ relations of experimental variables of Equation (2) and quantum chemical data on Equation (3) of fragment ions of substituted MTZ depending on sample type, scan number, and retention time; chemometrics.

4. Discussion

The rapid growth and discharge of industrial wastewater, furthermore, consisting of complex organic pollutants, is difficult to treat via traditional clean-up technologies of wastewater treatment plants. The metronidazone is among the widely used medications for treating bacterial infections. Its current ineffective treatment causes wastewater, which represents a serious environmental problem. The metronidazole is highly water-soluble and non-biodegradable. Thus, it easily accumulates and causes adverse effects on organisms. Thus, the effectiveness and safety of human health and environmental technologies for MTZ processing of wastewater emerge as crucial innovations. However, it is a challenging research area. Among various removal technologies, ozonation has gained considerable attention in wastewater treatment technologies. There are good oxidation capacity and the capability of improving the biochemical properties of MTZ in wastewater. In addition, there is a lack of secondary pollution. Despite the process suffering from problems. A certain selectivity occurs, causing for improvement of available catalytic reactions of ozonation. It is mostly used for oxidizing •OH-radical. Despite the high reaction efficiency, the ozonation process of MTZ shows a lack of oxidizing selectivity. This fact significantly challenges both the quantitative and structural analyses of the species as well as analyte reaction monitoring via mass spectrometric methods. Therefore, elaboration of innovative MS-based tools for precise, selective, sensitive, and accurate quantitative and 3D molecular structural determination of products of ozonation of MTZ in wastewater crucially contributes to developing effective clean-up technologies for MTZ removal. Such tools are of significant importance for fields of environmental chemistry and the establishment of effective programs for assessment of the risk for human health and the environment due to metronidazole pollution.

The stochastic dynamics mass spectrometric model Equation (2) has emerged as an exact tool for processing of MS measurable variables. It allows for exact quantitative analysis of species in environmental samples and biological fluids. It is complementary to Equation (3) and allows for simultaneous and exact 3D structural analysis of species, as well. The application of the novel approach to study MTZ in urine [14] has led to its exact quantification, and within the direct MS analysis. There is increased selectivity and specificity, as well. This study applies the innovative formulas to detail a case of analysis of metronidazole; however, in significantly complex conditions of ozonation reactions, which, as aforementioned, lack selectivity and have not been reported so far. The achieved superior performances compared with traditional approaches to both quantitative and 3D structural

MS-based analysis of MTZ derivatives provide fundamentally important support for a practical application of Equations (2) and (3) to determine analytes in real environmental samples and technological processes of ozonation of MTZ. Furthermore, there is a prospective application to an industrial scale, because the interaction of MTZ with O_3 results in high removal capacity, and, thus, it has direct technological implementation into wastewater treatment plant technologies. As detailed in the preceding subsections, the improved analytical methodology resulted in significantly enhanced analyte quantification performance, with |r| = 0.99983. Conversely, traditional approaches to process mass spectra and examining CID-MS/MS ions at m/z $136.931_2 \pm 2.828 \times 10^{-4}$ show |r| = 0.57656. The innovative Equation (2) and chemometric assessment of relation $D''_{SD} = f(\text{conc.})$ yield |r| = 0.99979. Thus, an exact quantification of metronidazole derivatives in a complex mixture of products of competitive oxidizing of organics. The improved performances affect not only the |r|-parameter, but also method selectivity and sensitivity. The utilization of Equation (2) for structural determination of analyte ions has yielded |r| = 0.93957. Therefore, Equation (2) allows for not only the exact quantification of the ozonation derivative of metronidazole, but also to determine precisely and selectively its molecular structure. This reliable knowledge permits further effective optimization of wastewater removal processes; furthermore, at an industrial scale, due to the fact that mass spectrometric methods are routinely used to monitor industrial-scale catalytic processes.

5. Conclusions

The powerful capability of the innovative stochastic dynamics model Equation (2) among various models for processing of mass spectrometric variables of exact quantifying and determining 3D structurally analytes is illustrated using metronidazol derivatives obtained due to ozonation. There is empirical evidence that the model Equation (2) is the only effective tool developed so far for processing exactly the fluctuations of measurands. In the case of metronidazole, a particularly challenging aspect is the fact that there is a lack of selectivity of the ozonation reaction, thus producing a set of competitive reactions. Despite this, there is a reinforced argument made in works employing model Equation (2) in studying biological fluids [14], environmental samples [15,20], and foods [58,59] that traditional concepts of processing measurands of analytes having low abundance peaks or are observed at low concentration should be used for semi-quantification. Conversely, model Equation (2) produces exact data on analyte quantity and its molecular structure. The latter task is carried out via a complementary employment in Equations (2) and (3).

The obtained novel results might be considered under the following three major points:

(1) The ozonization reaction of metronidazole produces N^3–OH derivative. Its mass spectrometric peaks have been quantified over a set of experimental conditions, and statistical significance has been evaluated via methods for chemometrics.
(2) Correlative analysis with performances via traditional approaches to process mass spectrometric variables; thus, examining the CID-MS/MS ion at m/z $136.931_2 \pm 2.828 \times 10^{-4}$ shows |r| = 0.57656, while the test of Equation (2) and assessment of relation $D''_{SD} = f(\text{conc.})$ causes for excellent performances (|r| = 0.99979);
(3) The structural analysis shows excellent correlation between theoretical D_{QC} parameters of Equation (3) and experimental MS parameters of intensity data (absolute intensity data or D''_{SD} parameters of Equation (2)) on analyte peaks; thus, achieving |r| = 0.93957.

These excellent results from studying very complex case of ozonation reaction of metronidazole as point (A)–(C) attempts to highlight return us to the starting point of the current study that Equation (2) is only currently available method for processing of mass spectrometric data and tackling fluctuations of low intensity analyte peaks which is capable for producing not only exact quantitative data on analytes, but also 3D molecular structural ones; furthermore, simultaneously. The achieved performances clearly highlight Equation (2) as a novel tool for not only prospective application to the fundamental analytical sciences, but also to the industry.

Supplementary Materials

The additional data and information can be downloaded at: https://media.sciltp.com/articles/others/2601211504245430/ACPA-25100104-SM-FC.pdf. Mass spectrometric, chromatographic data theoretical data (Figure S1–S8 and Tables S1–S9).

Funding

This research received no external funding.

Institutional Review Board Statement

Not applicable.

Informed Consent Statement

Not applicable.

Data Availability Statement

Experimental mass spectrometric raw data used in this study could be downloaded free of charge.

Acknowledgments

The author is grateful to Deutscher Akademischer Austausch Dienst, the Alexander von Humboldt Stiftung, and the Deutsche Forschungsgemeinschaft for various grants over the decades.

Conflicts of Interest

The author declares no conflict of interest.

Use of AI and AI-Assisted Technologies

No AI tools were utilized for this paper.

Abbreviations and Acronyms

ANOVA	Analysis of variance
AOPs	Advanced oxidation processes
BOMD	Born–Oppenheimer molecular dynamics
CBZ	Carbamazepine
CID	Collision-induced dissociation
DFT	Density functional theory
GS	Ground state
CQAs	Caffeoylquinic acids
MD	Molecular dynamics
MM	Molecular mechanics
MS	Mass spectrometry
MTZ	Metronidazole
QA	Quinic acid
RT	Retention time
SRM	Selected reaction monitoring
SMX	Sulfamethoxazole
TS	Transition state
WWPP	Wastewater processing plants
|r|	Correlation coefficient (absolute value)
r^2	Regression coefficient
sd(yEr±)	Standard deviation
se(yEr±)	Standard error

References

1. Beltran, F.; Jimenez-Lopez, M.; Alvarez, P.; et al. Kinetic modelling of ozonation and photolytic ozonation of metronidazole removal from water. *J. Ind. Eng. Chem.* **2025**, *144*, 654–662. https://doi.org/10.1016/j.jiec.2024.10.010.
2. Perez, T.; Garcia-Segura, S.; El-Ghenymy, A.; et al. Solar photoelectro-Fenton degradation of the antibiotic metronidazole using a flow plant with a Pt/air-diffusion cell and a CPC photoreactor. *Electrochim. Acta* **2015**, *165*, 173–181. https://doi.org/10.1016/j.electacta.2015.02.243.
3. Moslehi, M.; Zadeh, M.; Nateq, K.; et al. Statistical computational optimization approach for photocatalytic-ozonation decontamination of metronidazole in aqueous media using $CuFe_2O_4/SiO_2/ZnO$ nanocomposite. *Environm. Res*. **2024**, *242*, 117747. https://doi.org/10.1016/j.envres.2023.117747.
4. Gahrouei, G.; Vakili, S.; Zandifar, A.; et al. From wastewater to clean water: Recent advances on the removal of metronidazole, ciprofloxacin, and sulfamethoxazole antibiotics from water through adsorption and advanced oxidation processes (AOPs). *Environm. Res*. **2024**, *252*, 119029. https://doi.org/10.1016/j.envres.2024.119029.
5. Skalska-Tuomi, K.; Kaijanen, L.; Monteagudo, J.; et al. Efficient removal of pharmaceuticals from wastewater: Comparative study of three advanced oxidation processes. *J. Environ. Manag.* **2025**, *375*, 124276. https://doi.org/10.1016/j.jenvman.2025.124276.
6. Serna-Carrizales, J.; Zarate-Guzman, A.; Flores-Ramirez, R.; et al. Application of artificial intelligence for the optimization of advanced oxidation processes to improve the water quality polluted with pharmaceutical compounds. *Chemosphere* **2024**, *351*, 141216. https://doi.org/10.1016/j.chemosphere.2024.141216.
7. Available online: https://eur-lex.europa.eu/eli/dir/2024/3019/oj/eng (accessed on 27 November 2024).
8. Zhang, T.; Zheng, L.; Yang, X.; et al. Integrated spectral based monitoring, optimization and control of the combined ozonation and powdered activated carbon adsorption process to remove organic micropollutants from secondary effluent. *Water Res*. **2025**, *268*, 122588. https://doi.org/10.1016/j.watres.2024.122588.
9. Alhuwaymil, Z. Development, analysis, and effectiveness of an F-C-MgO/rGOP catalyst for the degradation of atrazine using ozonation process: Synergistic effect, mechanism, and toxicity assessment. *J. Environ. Manag.* **2025**, *374*, 123990. https://doi.org/10.1016/j.jenvman.2024.123990.
10. Ivanova, B. Special Issue with Research Topics on "Recent Analysis and Applications of Mass Spectra on Biochemistry". *Int. J. Mol. Sci.* **2024**, *25*, 1995. https://doi.org/10.3390/ijms25041995.
11. Prada-Vasquez, M.; Simarro-Gimeno, C.; Vidal-Barreiro, I.; et al. Application of catalytic ozonation using Y zeolite in the elimination of pharmaceuticals in effluents from municipal wastewater treatment plants. *Sci. Total Environ*. **2024**, *925*, 171625. https://doi.org/10.1016/j.scitotenv.2024.171625.
12. Janda, M.; Seah, B.; Jakob, D.; et al. Determination of abundant metabolite matrix adducts illuminates the dark metabolome of MALDI-mass spectrometry imaging datasets. *Anal. Chem.* **2021**, *93*, 8399−8407. https://doi.org/10.1021/acs.analchem.0c04720.
13. Ivanova, B. Stochastic dynamics mass spectrometric quantification and 3D molecular structural analysis of tricyclic antidepressant in marine dissolved organic matter. *Environ. Geochem. Health* **2025**, *47*, 211. https://doi.org/10.1007/s10653-025-02519-4.
14. Ivanova, B.; Spiteller, M. Exact quantifying of mass spectrometric variable intensity of analyte peaks with respect to experimental conditions of measurements—A stochastic dynamic approach. *Anal. Chem. Lett.* **2022**, *12*, 542–561. https://doi.org/10.1080/22297928.2022.2086822.
15. Ivanova, B. Stochastic dynamic mass spectrometric quantitative and structural analyses of pharmaceutics and biocides in biota and sewage sludge. *Int. J. Mol. Sci*. **2023**, *24*, 6306.
16. Ivanova, B.; Spiteller, M. A stochastic dynamic mass spectrometric diffusion method and its application to 3D structural analysis of the analytes. *Rev. Anal. Chem*. **2019**, *38*, 1. https://doi.org/10.1515/revac-2019-0003.
17. Ivanova, B.; Spiteller, M. Stochastic dynamic mass spectrometric approach to quantify reserpine in solution. *Anal. Chem. Letts*. **2020**, *10*, 703–721.
18. Ivanova, B.; Spiteller, M. Mass spectrometric stochastic dynamic 3D structural analysis of mixture of steroids in solution—Experimental and theoretical study. *Steroids* **2022**, *181*, 109001.
19. Ivanova, B.; Spiteller, M. Chapter 1: Mass spectrometric and quantum chemical treatments of molecular and ionic interactions of a flavonoid-O-glycoside—A stochastic dynamic approach. In *Advances in Chemistry Research*; Taylor, J., Ed.; NOVA Science Publishers: New York, NY, USA, 2022; Volume 74, pp. 1–126.
20. Ivanova, B.; Spiteller, M. Stochastic dynamic ultraviolet photofragmentation and high collision energy dissociation mass spectrometric kinetics of triadimenol and sucralose. *Environ. Sci. Pollut. Res.* **2023**, *30*, 32348–33237.
21. Ivanova, B.; Spiteller, M. Stochastic dynamic quantitative and 3D structural matrix assisted laser desorption/ionization mass spectrometric analyses of mixture of nucleosides. *J. Mol. Struct.* **2022**, *1260*, 132701.

22. Ivanova, B.; Spiteller, M. Electrospray ionization stochastic dynamic mass spectrometric 3D structural analysis of Zn^{II}-ion containing complexes in solution. *Inorg. Nano-Met. Chem.* **2022**, *52*, 1407–1429.
23. Ivanova, B. Structural analysis of polylactic acid in composite starch biopolymers—A stochastic dynamics mass spectrometric approach. *Innov. Discov.* **2024**, *1*, 26. https://doi.org/10.53964/id.2024026.
24. Ivanova, B. Stochastic dynamics mass spectrometric and Fourier transform infrared spectroscopic structural analyses of composite biodegradable plastics. *Pollut. Study* **2024**, *5*, 2741. https://doi.org/10.54517/ps.v5i2.2741.
25. Ivanova, B. Stochastic dynamics mass spectrometric structural analysis of nucleotides, *Adv. Anal. Sci.* **2024**, *5*, 3043. https://doi.org/10.54517/aas.v5i2.3043.
26. Ammar, H.; Brahim, M.; Abdelhédi, R.; et al. Enhanced degradation of metronidazole by sunlight via photo-Fenton process under gradual addition of hydrogen peroxide. *J. Mol. Catal. A Chem.* **2016**, *420*, 222–227. http://doi.org/10.1016/j.molcata.2016.04.029.
27. Höhn, D.; Renner, G. Small HRMS (Orbitrap) raw Files in Profile Mode for Fast Testruns of Processing Software [Data set]. Zenodo 2025. https://doi.org/10.5281/zenodo.15477095.
28. Frisch, M.; Trucks, G.W.; Schlegel, H.B. et al. *Gaussian 09*; Gaussian, Inc.: Pittsburgh, PA, USA, 2009. Available online: https://gaussian.com/gaussian16/ (accessed on 22 October 2025).
29. Dalton2011 Program Package. Available online: https://gitlab.com/dalton/dalton/tree/release/2020 (accessed on 22 October 2025).
30. Gordon, M.; Schmidt, M. Advances in electronic structure theory: GAMESS a decade later. In *Theory and Applications of Computational Chemistry: The First Forty Years*; Dykstra, C., Frenking, G., Kim, K., et al., Eds.; Elsevier: Amsterdam, The Netherlands, 2005; pp. 1167–1189.
31. Zhao, Y.; Truhlar, D. Density functionals with broad applicability in chemistry. *Acc. Chem. Res.* **2008**, *41*, 157–167. https://doi.org/10.1021/ar700111a.
32. Zhao, Y.; Truhlar, D. The M06 suite of density functionals for main group thermochemistry, thermochemical kinetics, noncovalent interactions, excited states, and transition elements: Two new functionals and systematic testing of four M06–class functionals and 12 other functionals. *Theor. Chem. Acc.* **2008**, *120*, 215–241. https://doi.org/10.1007/s00214-007-0310-x.
33. Hay, P.; Wadt, W. Ab initio effective core potentials for molecular calculations. Potentials for K to Au including the outermost core orbitals. *J. Chem. Phys*. **1985**, *82*, 299. https://doi.org/10.1063/1.448975.
34. Truhlar, D. A simple approximation for the vibrational partition function of a hindered internal rotation. *J. Comput. Chem*. **1991**, *12*, 266–270. https://doi.org/10.1002/jcc.540120217.
35. Wang, H.; Castillo, A.; Bozzelli, J. Thermochemical properties enthalpy, entropy, and heat capacity of C1–C4 fluorinated hydrocarbons: Fluorocarbon group additivity. *J. Phys. Chem. A* **2015**, *119*, 8202–8215. https://doi.org/10.1021/acs.jpca.5b03912.
36. Schleyer, P.; Schreiner, P.; Allinger, N.; et al. (Eds.) *Encyclopedia of Computational Chemistry*; Wiley: West Sussex, UK, 1998; Volumes 2 and 3, pp. 812–2300.
37. Schreiner, P.; Allen, W.; Orozco, M.; et al. *Computational Molecular Science*; Wiley: West Sussex, UK, 2014; Volumes 2 and 4, pp. 513–1257+1631–2523.
38. Allinger, L. Conformational analysis. 130. MM2. A hydrocarbon force field utilizing V1 and V2 torsional terms. *J. Am. Chem. Soc.* **1977**, *99*, 8127–8134. https://doi.org/10.1021/ja00467a001.
39. Burkert, U.; Allinger, N. *Molecular Mechanics in ACS Monograph 177*; American Chemical Society: Washington, DC, USA, 1982; pp. 1–339.
40. Miller, J.; Miller, M. *Statistics and Chemometrics for Analytical Chemistry*; Pentice Hall: London, UK, 1988; pp. 1–271.
41. Gao, S.; Zhao, Z.; Xu, Y.; et al. Oxidation of sulfamethoxazole (SMX) by chlorine, ozone and permanganate—A comparative study. *J. Hazard. Mater*. **2014**, *274*, 258–269. https://doi.org/10.1016/j.jhazmat.2014.04.024.
42. Magana, A.; Kamimura, N.; Soumyanath, A.; et al. Caffeoylquinic acids: Chemistry, biosynthesis, occurrence, analytical challenges, and bioactivity. *Plant J*. **2021**, *107*, 1299–1319. https://doi.org/10.1111/tpj.15390.
43. Can, Z.; Gurol, M. Formaldehyde formation during ozonation of drinking water. *Ozone Sci. Eng.* **2003**, *25*, 41–51. https://doi.org/10.1080/713610649.
44. Manasfi, T.; Houska, J.; Gebhardt, I.; et al. Formation of carbonyl compounds during ozonation of lake water and wastewater: Development of a non-target screening method and quantification of target compounds. *Water Res*. **2023**, *237*, 119751. https://doi.org/10.1016/j.watres.2023.119751.
45. Burkholder, J.; Cox, R.; Ravishankara, R. Atmospheric degradation of ozone depleting substances, their substitutes, and related species. *Chem. Rev*. **2015**, *115*, 3704−3759. https://doi.org/10.1021/cr5006759.
46. Lim, S.; Shi, J.; Von Gunten, U.; et al. Ozonation of organic compounds in water and wastewater: A critical review. *Water Res.* **2022**, *213*, 118053. https://doi.org/10.1016/j.watres.2022.118053.

47. Voukides, A.; Konrad, K.; Johnson, R. Competing mechanistic channels in the oxidation of aldehydes by ozone. *J. Org. Chem.* **2009**, *74*, 2108–2113. https://doi.org/10.1021/jo8026593.
48. Li, Z.; Xiang, L.; Pan, S.; et al. The degradation of aqueous oxytetracycline by an O_3/CaO_2 system in the presence of HCO_3^-: Performance, mechanism, degradation pathways, and toxicity evaluation. *Molecules* **2024**, *29*, 659. https://doi.org/10.3390/molecules29030659.
49. Ruffinoa, M.; Zanetti, M. Experimental study on the abatement of ammonia and organic carbon with ozone. *Desalination Water Treat.* **2012**, *37*, 130–138. https://doi.org/10/5004/dwt.2012.2780.
50. Hiserodt, R.; Pope, B.; Cossette, M.; et al. Proposed mechanisms for the fragmentation of doubly allylic alkenamides (tingle compounds) by low energy collisional activation in a triple quadrupole mass spectrometer. *J. Am. Soc. Mass Spectrom.* **2004**, *15*, 1462–1470. https://doi.org/10.1016/j.jasms.2004.06.009.
51. Adams, H.; Fanourakis, A.; Dahiya, A.; et al. Allylic amination of alkenyl alcohols: Simultaneous control of chemoselectivity and enantioselectivity in nitrene transfer using ion-paired catalysts. *ACS Catal.* **2025**, *15*, 14639–14646. https://doi.org/10.1021/acscatal.5c04140.
52. Goodson, D. *Mathematical Methods for Physical and Analytical Chemistry*; J. Wiley and Sons Inc.: Hoboken, NJ, USA, 2011; pp. 1–382.
53. Otto, M. *Chemometrics*, 3rd ed.; Wiley: Weinheim, Germany, 2017; pp. 1–383.
54. Taylor, J. *Quality Assurance of Chemical Measurements*; Lewis Publishers, Inc.: Chelsea, MI, USA, 1987; pp. 1–328.
55. Zeleny, R.; Harbeck, S.; Schimmel, H. Validation of a liquid chromatography-tandem mass spectrometry method for the identification and quantification of 5-nitroimidazole drugs and their corresponding hydroxy metabolites in lyophilised pork meat. *J. Chromatogr. A* **2009**, *1216*, 249–256. https://doi.org/10.1016/j.chroma.2008.11.061.
56. Council Directive 96/23/EC of 29 April 1996 on Measures to Monitor Certain Substances and Residues Thereof in Live Animals and Animal Products and Repealing Directives 85/358/EEC and 86/469/EEC and Decisions 89/187/EEC and 91/664/EEC. Available online: https://eur-lex.europa.eu/eli/dir/1996/23/oj/eng (accessed on 13 Decembre 2019).
57. Pandeti, S.; Feketeová, L.; Reddy, T.; et al. Nitroimidazolic radiosensitizers investigated by electrospray ionization time-of-flight mass spectrometry and density functional theory. *RSC Adv.* **2017**, *7*, 45211–45221. https://doi.org/10.1039/c7ra08312b.
58. Upadyshev, M.; Ivanova, B.; Motyleva, S. Mass spectrometric identification of metabolites after magnetic-pulse treatment of infected *Pyrus communis* L. Microplants. *Int. J. Mol. Sci.* **2023**, *24*, 16776. https://doi.org/10.3390/ijms242316776.
59. Motyleva, S.; Ivanova, B.; Vinokur, M.; et al. Gas chromatography–mass spectrometry analysis of carbohydrates and linoleic acid in tomato leaves depending on growing conditions: An experimental and theoretical study. In *Advances in Biology*; Grant, C., Ed.; Nova Science Publishers: New York, NY, USA, 2025; Volume 9. https://doi.org/10.52305/JDWC2175.